論文 / 著書情報
Article / Book Information

Title	Mechanism of Long-Term Excessive Deformation and Delayed Shear Failure of Underground RC Box Culverts
Authors	Maekawa, K., Zhu, X., Chijiwa, N., Tanabe, S.
Citation	Journal of Advanced Concrete Technology, Vol. 14, No. 6, pp. 183-204
Pub. date	2016, 5

Mechanism of Long-Term Excessive Deformation and Delayed Shear Failure of Underground RC Box Culverts

Koichi Maekawa, Xiaoxu Zhu, Nobuhiro Chijiwa, Shigeru Tanabe

Journal of Advanced Concrete Technology, volume 14 (2016), pp. 183-204

Scientific paper

Mechanism of Long-Term Excessive Deformation and Delayed Shear Failure of Underground RC Box Culverts

Koichi Maekawa[1*], Xiaoxu Zhu[2], Nobuhiro Chijiwa[3] and Shigeru Tanabe[4]

Received 27 November 2015, accepted 29 April 2016 doi:10.3151/jact.14.183

Abstract

The aim of this study is to clarify the mechanism of the progressive excessive deformation observed in real underground RC box culverts of about 30 years of age. It was found by the site-inspection, monitoring and the destructive testing that the excessive deflection of top slabs for the culverts, which is almost 10 times the design estimated value, accompanies the out-of-plane shear failure. It is also computationally investigated that the coupling of subsidence of the backfill soil and the combined creep and shrinkage of concrete after cracking is closely associated with the delayed shear failure found in the culvert in service. In order to prove the delayed shear failure under higher sustained loads, the time-dependent shear crack propagation was reproduced in the laboratory test and the computational approach used in this study was examined.

1. Introduction

Underground facilities which are essential parts of urban infrastructures are used for a wide range of applications from small pipelines for lifelines to middle and large-scale underground structures such as utility ducts and tunnels for transportation. As these facilities backfilled with soil can hardly be inspected visually, long-term serviceability and safety are an essential issue for durability design and maintenance.

In the past decades, the long-term monitoring data for cracking and deflection of underground RC utility ducts was reported (Kunieda *et al.* 2014) and the excessive deflection of top slabs of these box culverts was recognized as shown in **Fig. 1**. Although the deflection of the top slabs was not periodically measured, cracking and its width were inspected in 15 and 30 years after construction as shown in **Fig. 2**. Cracks were increasing in number and their width has been enlarged (Chijiwa *et al.* 2015). It means that the nonlinearity of the ducts has proceeded ahead in the past three decades, and it seems that the deflection might be multiplying as well. The cracks are dispersed over the bottom faces of the top slabs. Attention should be directed to the fact that large cracks are also seen at the box culvert's inside corner where the bending compression develops. Thus, these cracks are thought not to be caused by flexure. The diagonal shear cracks and out-of-plane failure were suspected in danger (Zhu *et al.* 2014).

It is hard to identify the mode of failure by naked eyes, because cracks can be seen only from inside of RC box culverts. Then, the authors conducted the non-destructive testing by using an ultrasonic device and finally picked up core-boring. The diagonal shear cracks were definitely found (Chijiwa *et al.* 2015). It is not known when this diagonal out-of-plane shear cracks appeared, but it is assumed as shown in **Fig. 2** that the shear failure may occur lately after the construction. In this paper, the authors define the late diagonal cracking as "delayed shear". Fortunately, the zone of shear failure is detected within the limited area, and the whole structural system remains stable at this moment.

It is indispensable to clarify the mechanics of delayed shear failure of RC culverts to predict what will take place in future. Otherwise, the maintenance planning cannot be systematically conducted. The aim of this study is to investigate the mechanism of long-term excessive deformation and possible time-dependent shear failure of underground RC box culverts. The authors reported the trial multi-scale analysis of the underground RC culverts to show the possibility of delayed shear failure by considering 1) subsidence of backfilled soil foundation, 2) differential shrinkage and 3) time-dependent crack propagation (Kunieda *et al*. 2014). This paper is to deepen the discussion in more detail with the step-by-step verification and to verify the multi-scale soil-RC interaction analysis as a tool for future design and asset management of underground urban infrastructures.

2. Multi-scale soil-RC interaction analysis

As underground box culverts are backfilled with soil, time-dependent creep of structural concrete before and after cracking has to be taken into account (Maekawa *et al.* 2008; Asamoto *et al*. 2006). At the same time, differential shrinkage of concrete is associated with

[1]Distinguished professor, The University of Tokyo, Japan. *Corresponding author,
E-mail: maekawa@concrete.t.u-tokyo.ac.jp
[2]Engineer, Shimizu Corporation, Tokyo, Japan.
[3]Associate Professor, Tokyo Institute of Technology, Tokyo, Japan.
[4]Chief engineer, Tokyo Electric Power Company Holdings, Inc., Tokyo, Japan.

long-term deformation and shear failure (Yoneda *et al.* 2013), because the inside space of box culverts is rather dry but their outer surface is surrounded by wet soil fundation and/or underground water. Since the out-of-plane shear failure is a problem in danger, the diagonal shear crack propagation, which is possibly associated with drying shrinkage of concrtete, shall be simulated (Gebreyouhannes *et al.* 2014) as well. Furthermore, the nonlinear soil-structure interaction is to be consiered for investigating the mecahnism of damages (Soltani and Maekawa 2015; Moshirabadi *et al.* 2015).

In this study, the authors utilize the thermo-hygral multi-scale analysis (integrated analysis) which may cover all factors stated in this chapter (Maekawa *et al.* 2008). The reliability, accuracy and scope of this simulation platform has been examined in the past decades based upon experimental facts and applied to some design and infrastructure maintenance for practice. First of all, further experimetal verification is caried out in terms of long-term structural performances of the underground box culverts.

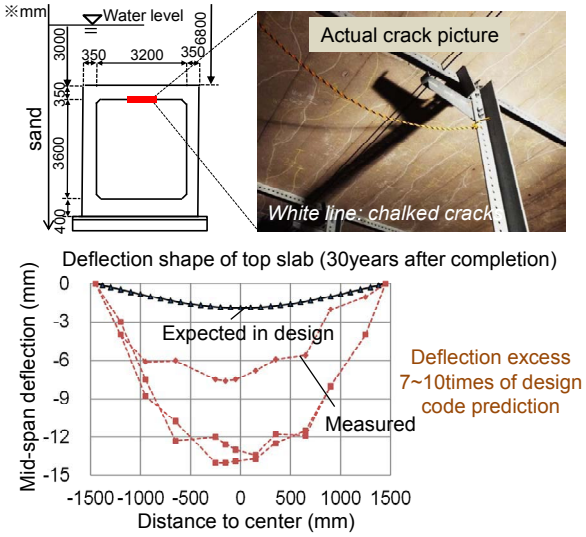

Fig. 1 Long-term excessive deflection with cracks of underground RC culvert (Kunieda *et al.* 2014).

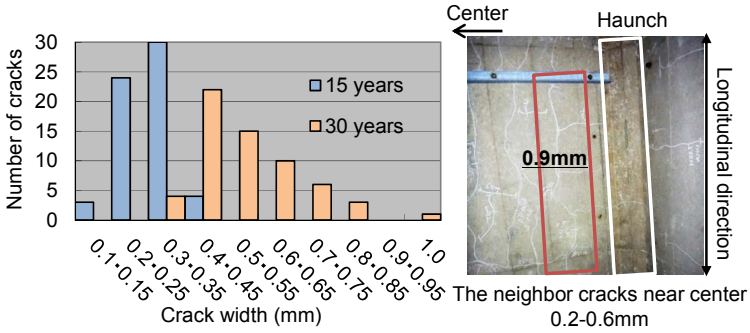

Fig. 2 The crack in progress and its large width observed near the corner haunch (Chijiwa *et al.* 2015).

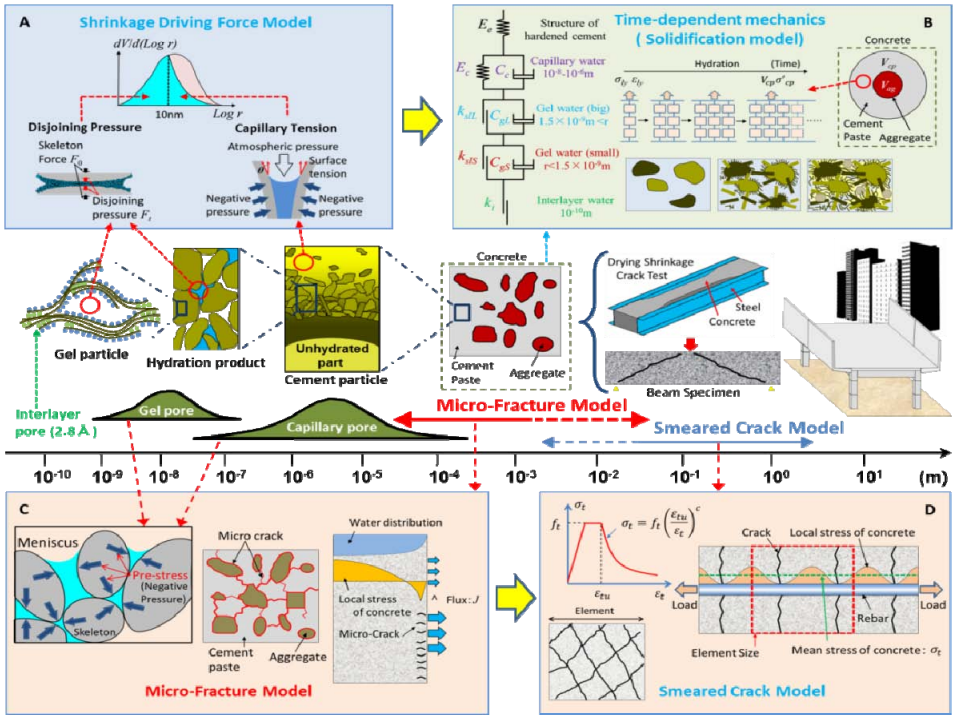

Fig. 3 Scheme of multi-scale modeling of structural concrete (Yoneda *et al.* 2013, 2015).

2.1 Vertical earth pressure to RC culvert backfilled with soil

The underground box culvert targetted in this study was constructed about 35 years ago by open-cut and cover construction system as shown in **Fig. 4**. After dumping disturbed soil backfilled between sheet piles and the RC culvert, the dead weight of the overlay soil was directly applied on the top slab of the box culvert. Here, it must be noted that the backfill soil may be consolidated by gravity and the earth pressure will be increasing. Dasgupta and Sengupta (1991) conducted the large-scale mock-up of the box culvert backfilled with soil and measured the earth pressure which increases more than the initial value (Bennet *et al*. 2005; Tadros and Benak 1989; Woodbury *et al.* 1926). As a matter of fact, any dumped soil more or less comes upon subsidence even after compaction works and the increasing earth pressure is a potential cause of the delayed shear failure concerned. Then, the computational scheme in this study is required to be able to simulate the soil-structure interaction in time domain.

The pre-analyses to target the trap door test (Kuwano and Ebizuka 2010) were conducted for experimental verification of the vertical soil pressure owing to differential settlement of soil. The overview of the test is shown in **Fig. 5**. This experiment is aimed to mechanically reproduce the deformational fields similar to the case of backfill soil's subsidence by using the trapdoors in downward motion, which is the analogy of the soil subsidence arround the box culvert and the rest of the fixed door represents the targetted underground box culvert. The motions of these trap doors were uniformly controlled by parallel rods connected to the single jack as shown in **Fig. 5**. The analysis domain was discretized by finite element mesh according to the shape and dimensioning of the set-up (lower right of **Fig. 5**). The same soil properties as those reported in the test were used in the nonlinear analysis as 0.652 of the void ratio, density=15.5 (kN/m^3), internal frictional angle=49 (degree), dilatancy angle=19(degree) and 0.95 of the relative density. As the dry sand was used, the cohesion strength is assumed to be zero. Joint interface elements are arranged between soil and concrete to allow shear slip, where the coefficient of friction is assumed to be 0.4. The constitutive model for soil used in this study was originally deveoped by Towhata and Ishihara (1985a, 1985b) and Gutierrez *et al.* (1993), and installed into the integrated analysis (Soltani and Maekawa 2015). The effect of creep and shrinkage of concrete (upper right of **Fig. 5**) will be also discussed in the following section.

Figure 6 shows the comparisons of experimental and analysis results. Just before the downward motion of the trap doors, the vertivcal soil presure applied on the flat floor was reported to be almost uniform as about 6 kPa, which is equivalent to the soil weight. After the trap door in motion, the soil pressure on the trap doors was decreasing. On the contrary, the pressure applied on the fixed floor was increased. The averaged pressure on the fixed floor came up to about 15 kPa and kept constant no matter how large the downward displacment was reproduced (left below of **Fig. 6**). It was also reported that the shear band was partially formed close to the fixed floor and roughly indicaed by dot lines.

This mode of deformation was simply illustrated in **Fig. 6** by Kuwano and Ebizuka (2010). It means that the shear stress along the shear band develops and that the resultant downward shear force along the shear band is applied to the fixed door together with the gravity action of the soil foundation. Then, the resultant soil pressure on the fixed floor (=analogy of the underground box culvert) become greater than the initial soil pressure.

The analysis results are indicated with the corresponding experimental measurement. In general, multi-scale integrated analysis used in this study is capable of reproducing the increased soil pressure on the stable door due to the downward displacement of the movable ones. Not only the rapid increase in soil pressure with relatively small downward displacement (maximum soil pressure is observed at 0.5mm displacement), but also the localized shear band (Soltani and Maekawa 2015), which has a strong relation with the mechanism of increasing soil pressure, can be well simulated. The magnification ratio of the increased soil pressure (>1) attributes to the negative friction which develops along the inclined shear band. It has been empirically reported to be 1.1~2.0 in accordance with the overlay depth to duct span ratio (Kuwano and Ebizuka 2010). Since the delayed shear failure is possibly associated with the soil subsidence, the authors decided to use this soil model in the integrated analysis.

2.2 Coupled differential shrinkage-swelling and sustained loads

As stated in Chapter 1, the time-dependent mechanics of concrete has much to do with the excessive deflection

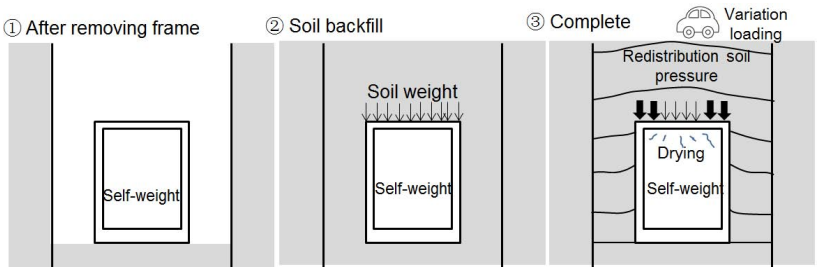

Fig. 4 Open-cut construction and consolidation of backfill soil after dumping.

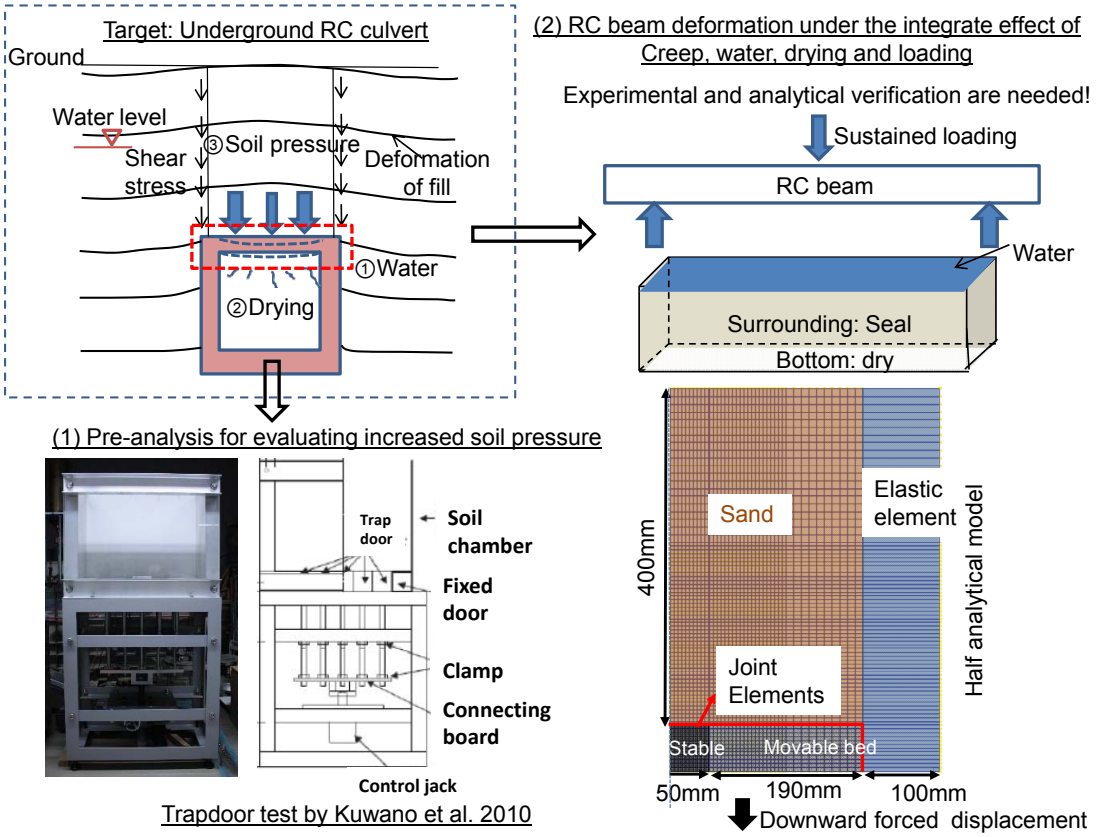

Fig. 5 Vertical soil pressure by trapdoor test (Kuwano and Ebizuka 2010) and finite element discretization.

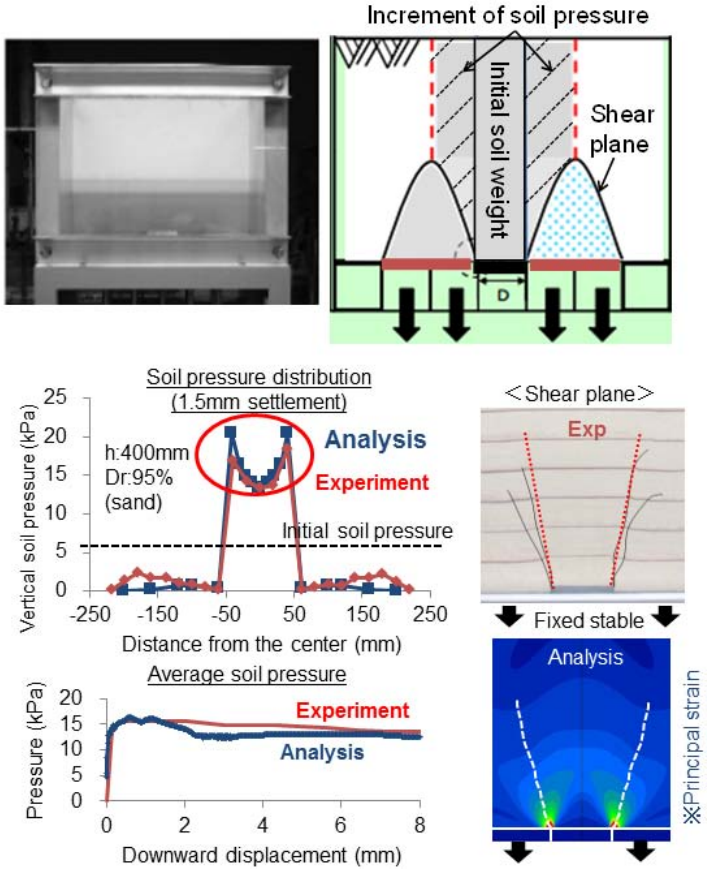

Fig. 6 Distribution and transition of vertical soil presure under the downward displacement of trapdoor.

and the delayed shear failure of underground RC culverts. In design of RC members, the effects of creep and the shrinkage has been estimated seperately, and the whole structural responses were assumed to be a simple summation of each response. However, the reality of drying concrete deformation under the sustaind stress is not the mere summation of the one of wet concrete under sustaind stress (basic creep) and the volume change of drying concrete of zero stress (drying shrinkage). This is called as Pickett effect (Pickett 1942; Bazant 2001).

This nonlinearity is consistently simulated in considering moisture transport and the constitutive model for cement paste of meso-scale (Asamoto *et al*. 2006) before and after cracking (Maekawa *et al*. 2008; Yoneda *et al*. 2014, 2015). The coupling of sustained stresses and drying was also found to cause an excessive deflection of long-span PC box sectional viadcuts of about 10 years after construction (Bazant *et al*. 2010; Ohno *et al*. 2012). The authors also assume that the same coupling problem would be one of possible causes of excessive deformation and delayed shear failure as well. The excessive deflection of the PC viaducts and their simulation are mechanically related to strucrtural concrete before cracking. But, the problem of the underground RC box culverts discussed in this study is the one after cracking.

For verifying the integrated model used in this study, the authors carried out the beam tests under sustained loads subjected to the gradient of the moisture as shown in the middle of **Fig. 7**. Four slender beams of different ambient moisture states denoted by N, W, P and A (See **Table 1**) were prepared and simply supported at both ends of the beam. Then, the shear deformation and out-of-plane failure are negligible. The concentrated dead weight of steel bars was put on the span center of 6.0m as shown in **Fig. 7**, and the time-dependent deflection was measured periodically. Within the rectangular section of 18*30cm, three D16 deformed bars were arranged as flexural main reinforcement with the effective depth of 15.0cm.

Four different moisture related boundary conditions were reproduced as listed in **Table 1** and illustrated in the upper and the lower of **Fig. 7**. Specimen N is the standard case where the moisture loss by drying was allowed from all faces of the specimen after 9 days curing with the wooden formwork. After 281 days, the top face was covered by the stagnant water by a framed pond (illustrated in blue face of **Fig. 7**) and consequently, the swelling of concrete took place. This case is intended to examine the model of swelling concrete associated with water pre-wetting. As a matter of fact, the underground RC culverts are subjected to seasonal drying and wetting.

After 9 days curing like Specimen N, all side faces of Specimens W, P and Specimen A were sealed with sili-

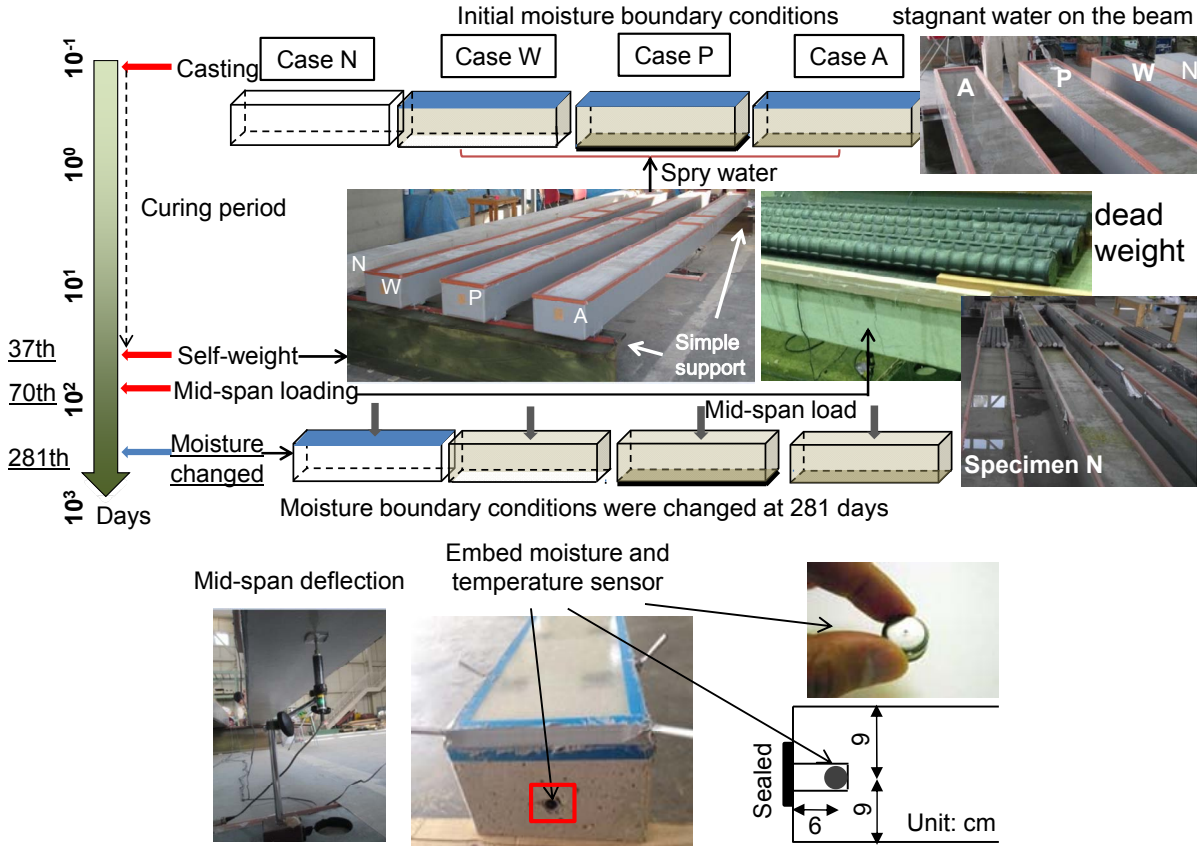

Fig. 7 The slender beam specimens under different boundaries of moisture.

Table 1 Specimens' boundary conditions.

Specimen	Mid-span Loading	Water conditions on the top surface		Sealed conditions	
		Before 281day	After 281day	Sides	Bottom
N	1.0kN	No	Yes	No	No
W		Yes	No	Sealed	No
P				Sealed	Sealed
A					

*Specimen P and Specimen A are sealed by epoxy grout and the polystyrene sheet, and polyurethane lining, respectively in order to check and compare sealing performances as shown below.

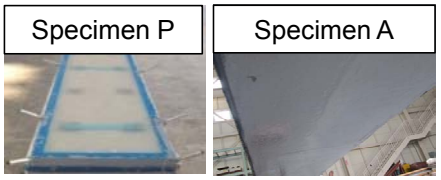

cone to reproduce moisture motion in one-direction. The bottom face of Specimen W was kept without sealing and exposed to room air. The bottom face of Specimens P and A were sealed by using different materials. Specimen P was sealed with the epoxy grout and the polystyrene sheet (see **Table 1**). Specimen A was sealed with polyurethane lining. The reason why the authors tried these methods of sealing in practical use is to multiply examine the perfectness of moisture sealing. If both materials would have the same performances, Specimen P and Specimen A shall behave similarly. Specimens W, P and A were targeted so that the differential shrinkage is coupled with the sustained flexure with cracking. This situation is also thought to be similar to the problematic top slabs of large numbers of cracks. The moisture sensors were embedded inside the specimens (See the lower center of **Fig. 7**) to check the transient states of moisture over the 18cm depth direction of the specimens.

After the simple support of Specimens W, P and A, water was given the top concrete surface. **Figure 8** shows the time-dependent deflection of these specimens. At the very beginning, the upward deflections of the three specimens were almost the same as about 2mm, because the water was absorbed from the top concrete surfaces and the drying shrinkage deformation of concrete was rapidly recovered and the upper flange of RC beams expanded. After the water was charged, the four specimens deformed subjected to the self-weight. Since the internal water content were different, the creep rate of Specimen N is relatively greater than the other three wet cases of Specimens W, P and A.

About one month after the water charge, a sustained loading with 1.0kN weight was carried out at the mid-span of all four slender RC beams. The deflection increased instantaneously at this time. Under the effect of self-weight and mid-span sustained loading and drying shrinkage propagating, time-dependent creep deflection proceeded. The creep rate and the deflection of Specimen N is quite larger than the cases of W, P and A. It is noticed that time-dependent creep deflections of Specimen W, P and A just developed at the beginning of loads, and converged to the stability. It can be proved that lack of water could accelerate creep rate. By supplying water to the compression zone to reduce the drying shrinkage and to increase water content, the creep deflection can be effectively controlled in thermo-mechanical point of view.

When 281 days passed after loading, the moisture states of the four specimens were reversed. Water was given the specimen N which had been dried. The water stored on the top surface of Specimen W, P and A was conversely removed. An instantaneous jump of upward deflection was observed for Specimen N. This is similar to the cases of W, P and A when water was sprayed to the flexural compressive side. This is because the drying shrinkage at the bending compression side was suddenly recovered because of water absorption and compression flange expanded. On the other hand, the creep deflection of Specimens W, P and A was suddenly increased because the water content was reduced and drying shrinkage conversely propagated after the removal of water.

The deflection of Specimens P and A is smaller than the case of W under the same loading and the ambient conditions. This is because the side and bottom faces of Specimen P and Specimen A are sealed so that it is more difficult for water to escape from concrete to atmos-

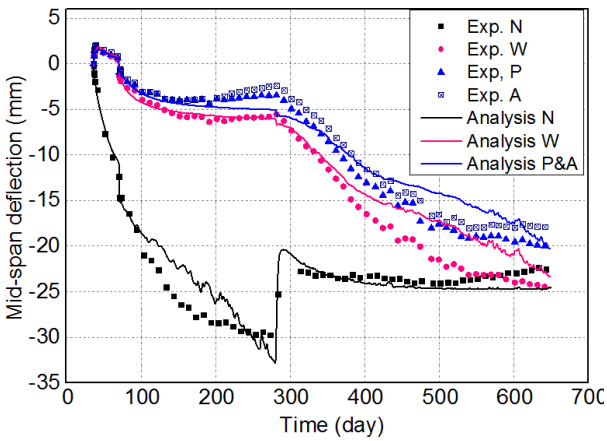

Fig. 8 Analytical and experimental deflection of four specimens.

Table 2 Mix proportion of concrete used.

W/C (%)	water (kg/m^3)	cement (kg/m^3)	gravel (kg/m^3)	sand (kg/m^3)	air (%)
62.6	164	262	1082	845	4.5

Table 3 Material properties measured and used in the analysis.

Concrete compressive strength	Steel yield strength	Bending failure load
24 N/mm^2	409 N/mm^2	17.7 KN

phere. That is to say, the moisture can be fairly kept in Specimen P and Specimen A, whose side faces and bottom ones are sealed. The way of the side sealing of the Specimens P and A is common with silicon. The bottom sealing effect of Specimen A seems a little better than Specimen P, because the deflection of Specimen A is lightly smaller than Specimen P.

For experimental verification of the multi-scale integrated analysis used, time dependent creep deflection of four beams with bending cracks was computed as shown in **Fig. 8**. **Figure 9** shows the FE discretization and the mix proportion and the material properties were used for input information of the integrated thermodynamics (Maekawa *et al*. 2008, Maekawa and Ishida 2002) As the moisture migration is in one-way and wetting/drying is defined on the upper and lower faces of the section, comparatively smaller size of elements is specified and the mean sizes of the elements placed around the core of the section are about twice the average size of coarse aggregates in consideration of moisture migration analysis and local moisture exchange between aggregates and surrounding cement paste phases (Yoneda *et al*. 2014). Here, the cement hydration just after the mixing and associated micro-structure formation was computed in time and space, and the time-dependent deformation of cement hydrates were simulated with the moisture states kept in the formed micropores. Thus, the mix proportion of concrete (see **Table 2**) is used as the input data of this thermo-mechanics integration. After cracking of hardened concrete, multi-directional crack (Maekawa and Fukuura 2014) and the meso-scale models were combined to conduct the behavioural simulation. The properties of materials used and the bending capacity calculated by the design formulae of in-plane theory are summarized in **Table 3**. Thus, the applied sustained load level is less than 10% of the bending capacity of the specimens, and the short-term material nonlinearity is much less. The time-dependent deflection of beams and slabs under room ambient states were studied (Guo and Gilbert 2002; Gilbert 1999), and the simulation by the integrated analysis has been verified (Maekawa *et al.* 2008). This study is further to examine the applicability under strong gradient of moisture profile with exposure to condensed water.

The room temperature and the relative humidity were measured every one hour for about two years as shown in **Fig. 10**, which includes one-day averaged values used for the boundary conditions of the integrated analysis. **Figure 11** shows the measured and analysed temperature and the relative humidity inside the specimens. Except for the specimen N, the internal relative humidity is

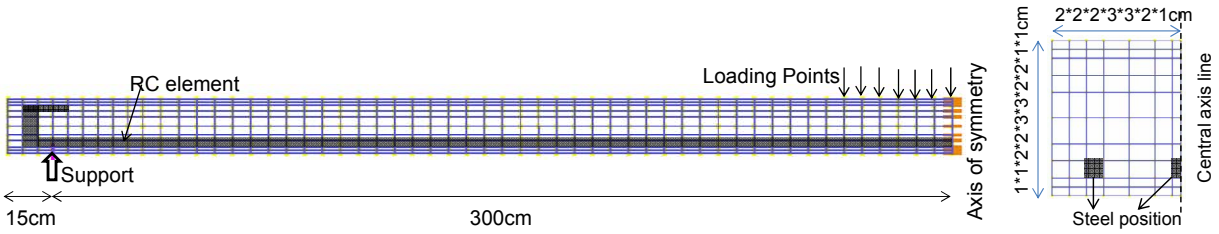

Fig. 9 Analytical model of RC beams.

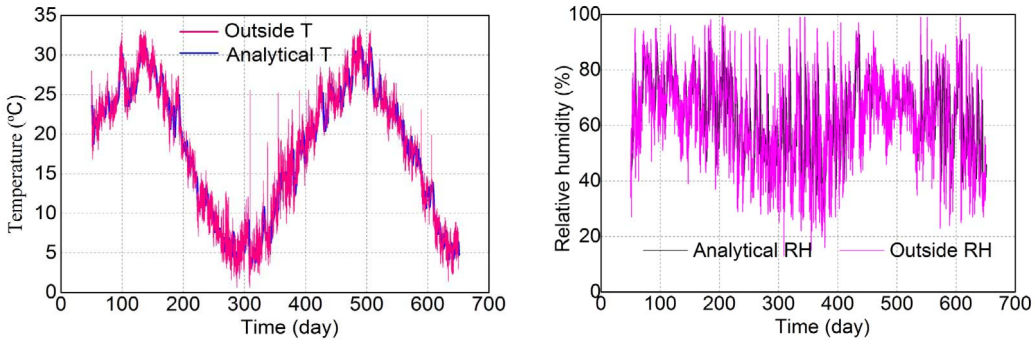

Fig. 10 Ambient temperature and relative humidity and those used for themo-hygral analysis.

higher than the ambient state owing to the moisture supply from the top surface of the specimen. The simulated deflection as well as the micro-climate is not so far from the reality within the reasonable accuracy for practical use.

3. Site inspection and destructive testing

As discussed in the previous chapters, the computational tool is ready to simulate the long-term multi-scale behaviors of the underground culverts with the excessive deflection. Here, the states of constituent materials and magnitude of deterioration of the targeted culverts shall be clarified because more than 30 years have passed after construction. Then, the authors made the detailed visual inspection in terms of cracking, laser measurement of the internal space (nearly equal to the deflection of the top slab), core sampling of concrete and the destructive testing for working stresses of reinforcing bars.

Figure 12 shows the mid-span deflection and the location of cracks. First, the absolute distance between the top and the bottom slabs was measured by the laser scanning devices. The relative distance compared with the one at the corner edges of the box section was calculated. Unfortunately, the initial distance just after the construction is not available. Then, the authors assume that the top slab would be constructed being in flat plane. Then, the relative distance might be close to the deflection after the construction. This measurement is much larger than the one calculated by the RC in-plane theory. In fact, some bolts and steel devices, which were attached to inside of the culvert, were found to be buckled and ruptured. The cracks indicated in red lines in **Fig. 12** were found at the 30 years inspection, and the rest of the cracks were recorded at 15 years inspection. Then, it can be said that large number of cracks were further produced between 15 and 30 years of age.

As the excessive soil pressure as discussed in Chapter 2 is likely to introduce the yield of main reinforcement which would result in larger deflection than expected, the destructive testing of working stresses for reinforcement was carried out (see **Fig. 13**). First, the con-

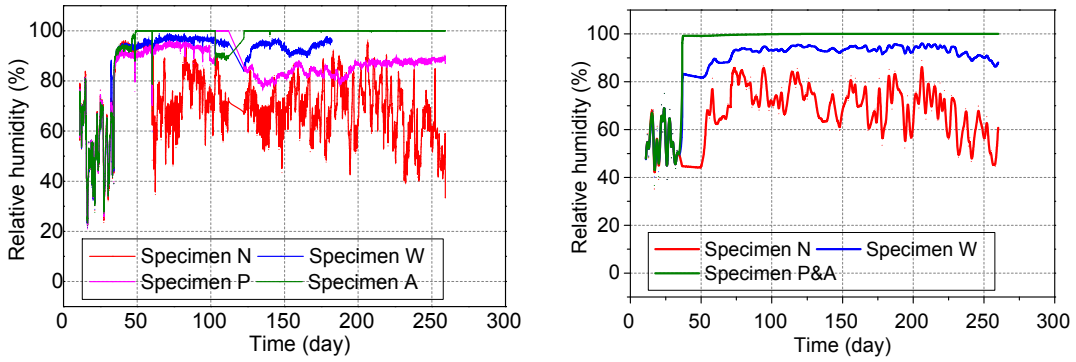

Fig. 11 Moisture histograms inside of the hollow core: measurement (left), analysis (right).

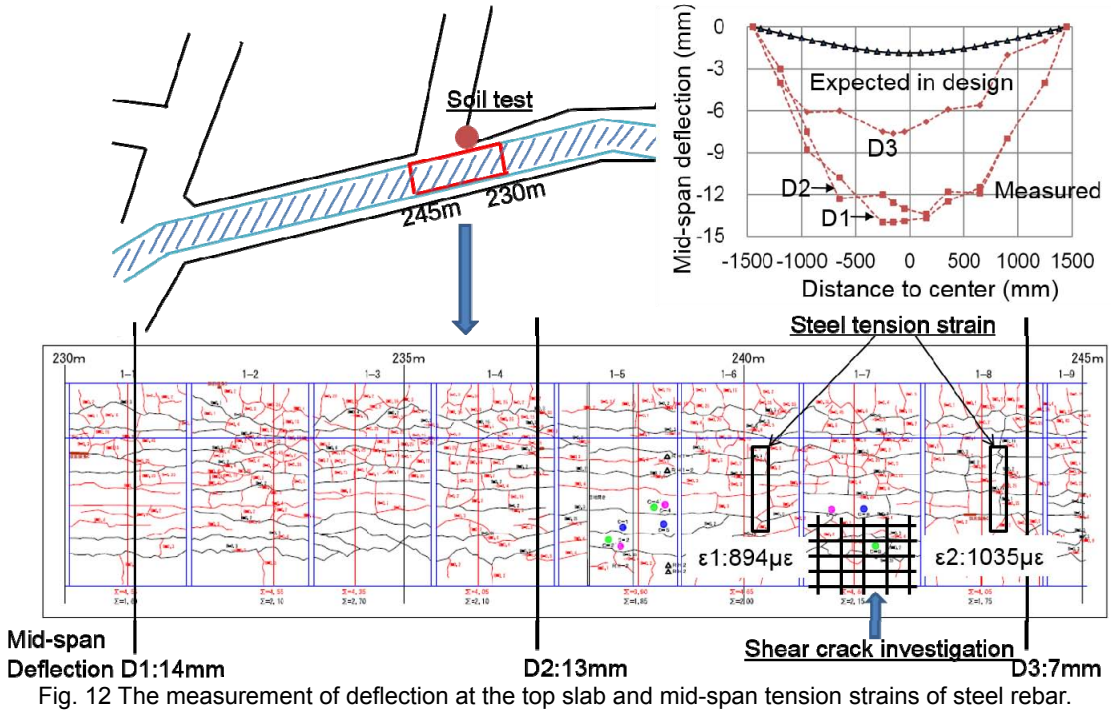

Fig. 12 The measurement of deflection at the top slab and mid-span tension strains of steel rebar.

crete cover was removed after the strengthening of the neighboring concrete and second, the strain gauges were put on the surface of reinforcing bars. Third, the steel bars with the gauges were cut at both ends and taken off from the main body of the RC box culvert. The steel stress was completely released and the elastic recovery to represent the working stress was measured as shown in **Fig. 14**. The so-called release test which the authors used in this study has been applied to PC viaducts (Maruyama 2007) and RC piers (Osada *et al*. 2006) to check the structural soundness as well.

The underground RC culverts are located about several meters deep beneath a narrow lane in a suburban area. Then, heavy truck and vehicles could not pass. In the past decades, no great earthquake actions happened to this area, too. Furthermore, the traffic loads can be dispersed widely and its impact to the underground culvert is much small. Thus, it can be assumed that live load's effect of traffics is negligible on the excessive deflection discussed in this paper. Other underground RC culverts were also inspected widely in several towns in Japan and the authors could discover the same excessive deflection and lots of cracks. Then, this type of damage of urban underground facilities is regarded as a risk factor in the future asset management.

According to the yield strength of reinforcing bars, the elastic strain limit is about 1,800μ. The strain recovery of all points along the bar is less than the yield strain limit. Then, it can be concluded that the working stress of main reinforcement has been less than the yield strength of steel and kept in elasticity. So, the excessive deflection and the large numbers of cracks cannot be explained by the inelasticity of the structures. The working stress level is about 1/2 of the yield strength. These culverts were originally designed based upon the allowable stress method where the safety factor of the reinforcement was 3. If the earth pressure wouold be equivalent to the the overlay soil, the working stress of reinforcement is expected to 1/3 of the yield strength. One of the possible reasons of this mismatching of the stress level is that the real earth pressure is 1.5 time larger than the design earth pressure due to the subsidence of the backfill soil as discussed in Section 2.1.

The concrete core samples were also collected and the compressive strength was measued as shown in **Table 4**. The mix proportion and the composition of concrete were examined as well. The strength development of structural concrete is sufficient. Although the concrete quality is not so high in view of durability, the authors could not find any corrosion of steel in concrete. Then, the excessive deflection cannot be attributed to the aging of constituent materials.

4. Multi-scale thermo-mechanics analysis

This chapter is to simulate the long-term deformation and failure of the underground box culverts by using the multi-scale integrated analysis. These functions have been examined beforehand on soil subsidence (section 2.1) and the differential shrinkage (section 2.2) with sustained stresses before and after cracking. In order to upgrade the reliability of the analysis, the authors conducted the in-situ boring test of foundation as shown in **Fig. 15**, and used the tested properties of soil (see **Table 5**) for the integrated analysis.

In order to enhance the reliability of the integrated analysis, the relative humidity inside the structural concrete was measured at site by digging the bore-holes as shown in **Fig. 15**. The temperature and moisture sensors were set up inside the holes 5cm from the surface and measured for a couple of months. The relative humidity of concrete just close to the outer surface (No.1-2, No.2-2 in **Fig. 15**) was almost 100% as shown in **Fig. 16**. For conducting the integrated analysis, we can define the perfectly wet boundary condition of the outer surface. The ambient humidity inside the box culvert was fluctuating by air conditioning in between 20 and 40%, but the relative humidity of the micro pores of concrete near the internal surface was almost kept constant as 60%. Then, 60% relative humidity was defined as the other boundary condition for the integrated analysis. The temperature varied rather stably around 25 degree. Then, the constant temperature of all surfaces (25 degree) was assumed in the analysis.

The integrated analysis was performed for life assessment of the RC culvert whose finite element discretization of 2D one-half domains is shown in **Fig. 17**. The space-averaged smeared crack and reinforcement modeling is used and the bond between concrete and reinforcement is expressed by means of the tension stiffness formulation for post-cracking states (Vecchio and Collins 1986; Salem and Maekawa 1999). As the steel arrangement pattern is not uniform in the longitudinal direction of the culvert, the averaged reinforcement ratio was used for 2D analyses. The wet and dry ambient conditions were defined as stated previously. The wet curing of concrete was assumed for 28 days during which the sealed condition is set forth in the integrated analysis. For reproducing the impact of consolidation, the forced downward displacement was made at the bottom line of backfill soil like the trapdoor test as shown in **Fig. 5**. Since the subsidence of the backfill soil is thought to take place and converge earlier rather than the concrete creep and drying shrinkage (Bang *et al*. 2007; Lade and Liu 1998; Siddiquee *et al*. 2006), the forced displacement increment was made constantly for 2 days. After the termination of consolidation, just the dead weight was continuously applied. According to the soil boring test, the shear stress-strain relation of soil under the confinement σ_c'=98kPa is specified as shown in **Fig. 17**.

To figure out the effects of the soil subsidence and differential drying shrinkage and creep on the long-term deflection and shear failure of the top slab, the following four sensitivity analyses are executed; Case I: no drying of concrete and no subsidence of soil, Case II: subsidence with no drying, Case III: drying but no subsidence and

①Reinforced with carbon fiber sheet

②Remove surface concrete; attach strain gauge; measurement started

③Cut steel rebar by disk sander

④Steel condition after cutting

⑤Concrete chipping

⑥Take off the steel rebar
Measurement finished

⑦Steel rebar restoration

⑧Surface recovery

Fig. 13 Tension steel strain measurement process.

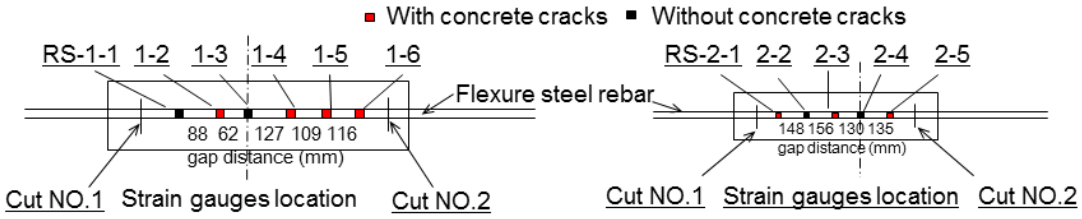

Step	Time	steel cut test 1						steel cut test 2				
		RS-1-1	1-2	1-3	1-4	1-5	1-6	RS-2-1	2-2	2-3	2-4	2-5
Initial	15:45	0	0	0	0	0	0	-1	0	0	0	0
Left cut start	15:45	0	0	0	0	0	0	-1	0	0	0	0
Left cut end	16:08	-890	-760	-580	-500	-250	-400	-941	-744	-574	-396	-318
Right cut start	16:11	-890	-760	-585	-550	-250	-420	-939	-744	-576	-398	-318
Right cut end	16:22	-890	-800	-650	-650	-700	-620	-955	-804	-755	-741	-768
Concrete cut start	16:25	-890	-805	-650	-650	-700	-620	-955	-804	-755	-741	-762
Concrete cut end	16:39	-894	-890	-885	-820	-800	-800	-969	-995	-1039	-853	-735
Final	16:39	-894	-890	-885	-820	-800	-800	-967	-988	-1035	-852	-735

The measurement of strain gauge(με, -:compression)

Fig. 14 Measurement of elastic strain recovery of reinforcing bars (minus value).

Table 4 Concrete material tested results compared with design values.

	Investigation	Design
compression strength (MPa)	24.2	24
Young's modulus (MPa)	16.6	25
cement (kg/m^3)	393	285
water (kg/m^3)	248	154
fine aggregates (kg/m^3)	643	809
coarse aggregates (kg/m^3)	976	1076
water cement ratio (%)	63	54
carbonation depth (mm)	29.2	concrete cover:58.6

Table 5 Soil foundation investigation test data.

Sample	A	B
wet density (g/cm^3)	1.923	1.783
dry density (g/cm^3)	1.496	1.349
soil density (g/cm^3)	2.68	2.696
water content (%)	28.5	32.2
void ratio	0.792	0.998
saturation ratio (%)	96.6	87
average N-value	2	0
cohesive force (KN/m^2)	3.2	9.6
internal friction angel (°)	34.7	32.3

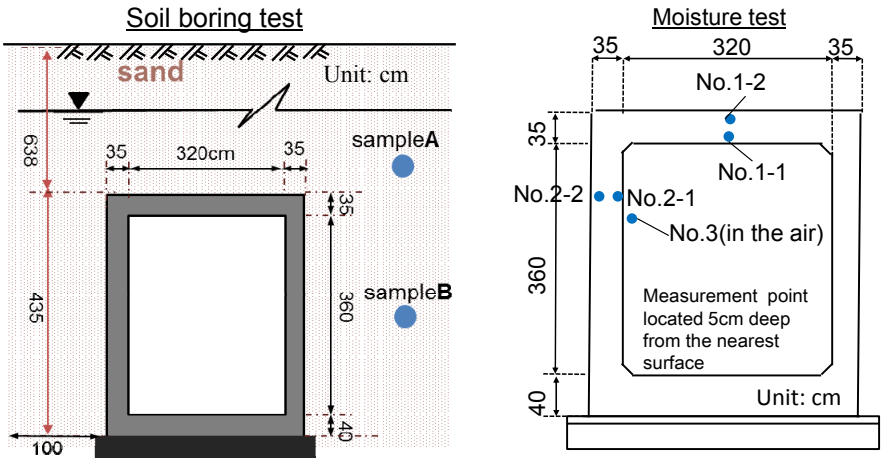

Fig. 15 The location of soil and moisture measurement.

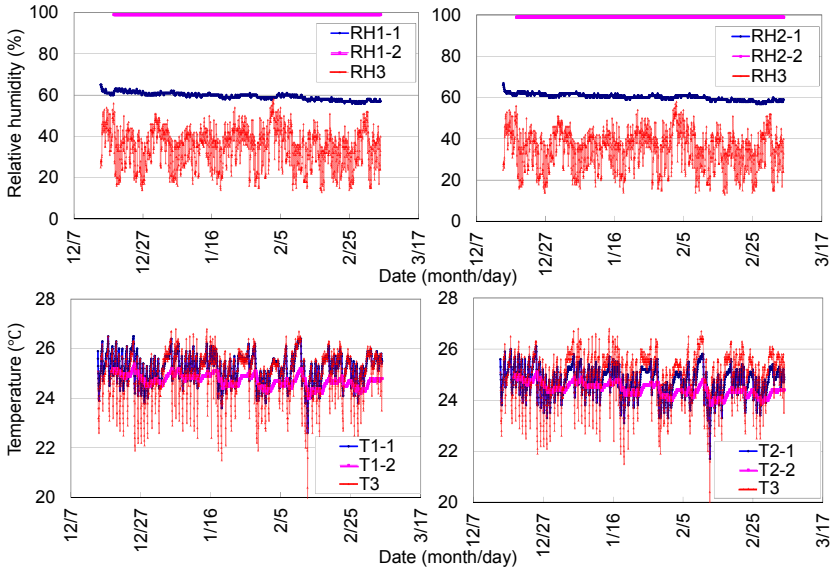

Fig. 16 The measured relative humidity and the temperature inside the concrete.

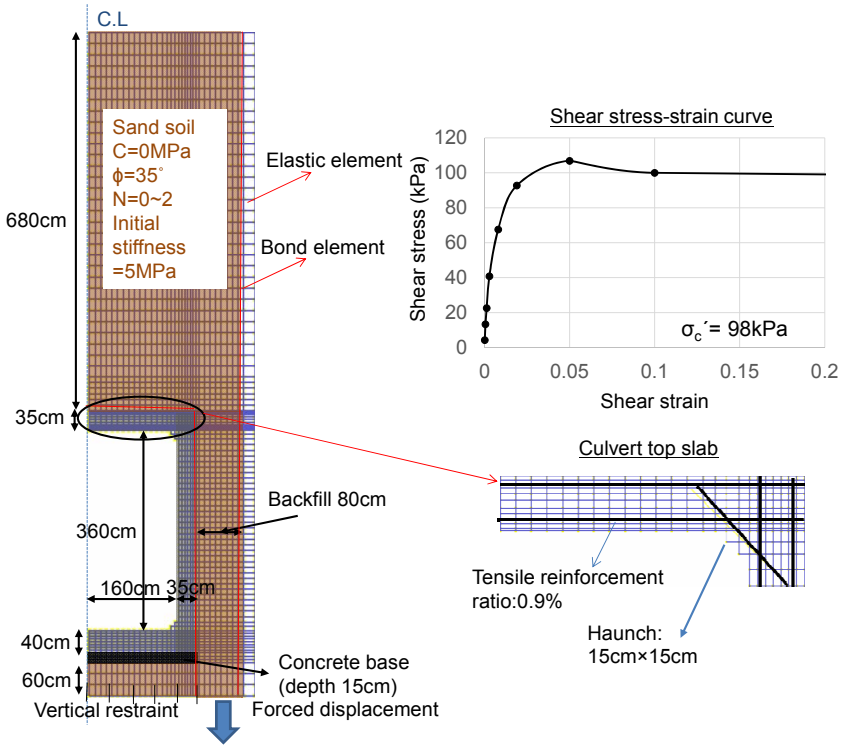

Fig. 17 Two dimensional model of the underground RC culvert.

Case IV in consideration of all factors as the most realistic case as shown in **Fig. 18**. Thus, the difference between Case I and Case II, III, IV respectively represent each effect described above. In reference to the site-monitoring as shown in **Fig. 16**, the ambient temperature and the relative humidity of Case III and Case IV were simply maintained at the annual averages (inside culvert: 25 ℃ RH 60%, outside: 20℃ RH 100%).

In Case II and IV, the large subsidence of the backfill soil, which may induce the maximum possible soil pressure (see **Fig. 6**), was intentionally produced. The effect of the increased earth pressure due to the consolidation of backfill is thought to be somewhere in between the two extreme cases of Case I and IV. **Figure 18** shows the deflection computed for 4 cases. The most realistic case of IV indicates the predicted deflection, which is close to the reality of site-measurement, and much larger than the case-I, which is equivalent to the structural design case for practice. The excessive deflection can be reproduced in the multi-scale integrated simulation, and the strain of main reinforcement is fairly predicted as well. In both computation and the reality, no yield of reinforcement takes place despite of the large deflection.

The influence of the differential shrinkage of concrete can be seen by comparing Case I (no shrinkage, no soil consolidation) with case III. Both flexural and shrinkage cracks computationally take place on the tension side of the top slab accompanying the reduced flexural stiffness. But, in both reality and simulation, no yield of reinforcement occurs and the earth pressure hardly changes (see **Figs. 18** and **19**). Anyhow, effect of shrinkage and creep cannot be a sole reason of the excessive deflection.

The effect of backfill soil subsidence can be checked by comparing Case I and Case III of no drying shrinkage. The uneven settlement of the side backfill causes additional soil pressure like the case in **Figs. 5** and **6**. Consequently, the soil pressure on the top slab and the stress of main reinforcement increases about 1.5 times. Then at the early age when the soil pressure becomes stable, the deflection becomes about 1.5 times large. After that, almost the same rate of deflection proceeds as that of Case I as shown in **Fig. 18**. In reality, the stress level of flexural tension reinforcement is on the similar magnitude to the computed one (see **Fig. 14**). Then, it can be concluded that the soil subsidence cannot be a unique reason of the excessive deflection.

The simple summation of Case II and Case III is indicated by dotted line in **Fig. 18**. This fictitious line does not reflect the nonlinear interaction of creep and shrinkage. This trend denoted by the dotted line is almost the same as the full nonlinear analysis of Case IV up to 1~2 days, because the drying shrinkage is almost nil. Afterwards, the deflection by the full analysis of Case IV gradually deviates from the dotted line of the simple summation of individual impact of creep, shrinkage and the soil subsidence up to 100~300 days after the loading. Here, attention shall be directed to 300~500 days after which the rate of deflection by the full analysis Case IV is greatly accelerated, and the absolute deflection comes up to 10~20 times the one of Case I. As a matter of fact, the computed deflection around 30 years of age is almost similar level to the real deflection, although the deflection at each location has some scatter as shown in **Fig. 12**. In consideration of the possible deviation of the

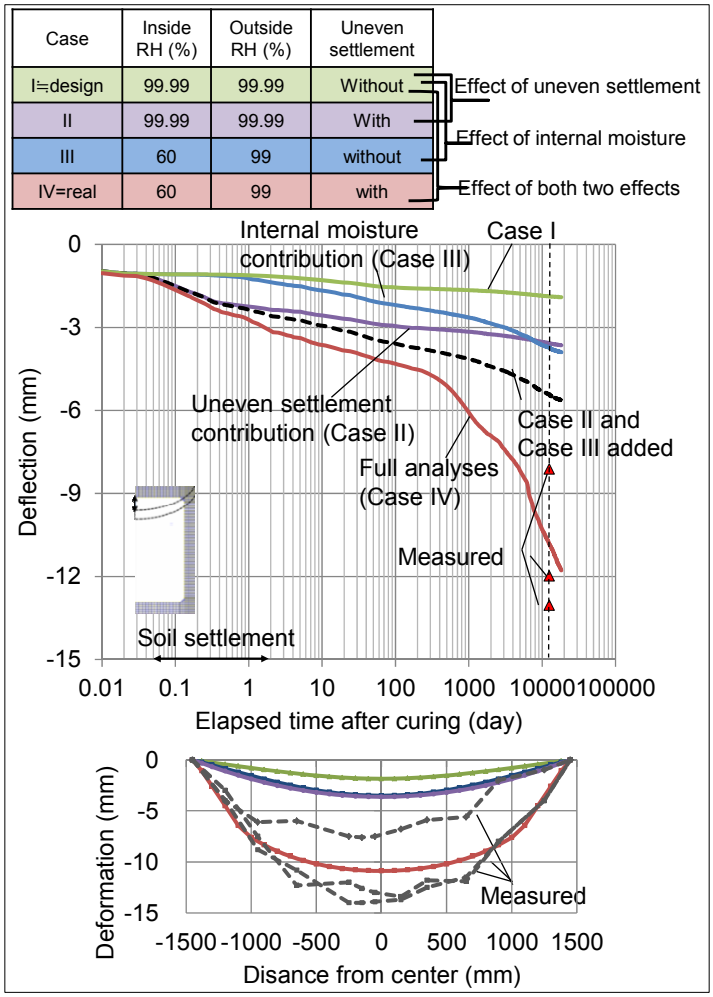

Fig. 18 Long-term deflection at mid-span and deformational mode at current age.

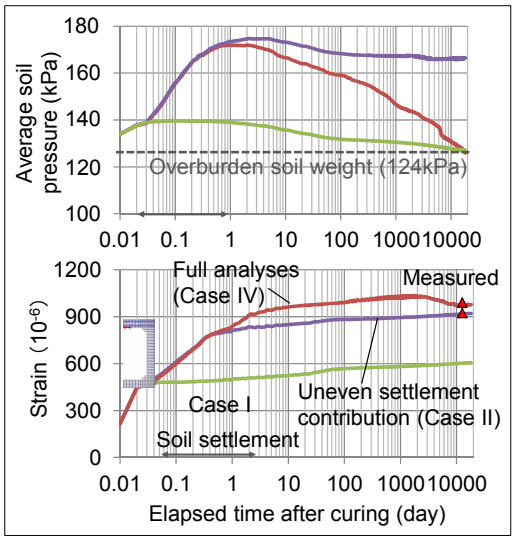

Fig. 19 Tension steel strain at mid-span with average vertical soil pressure on culvert.

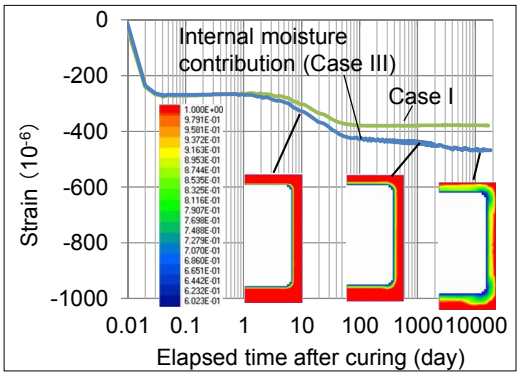

Fig. 20 Compressive steel strain at mid-span with internal RH contour figure.

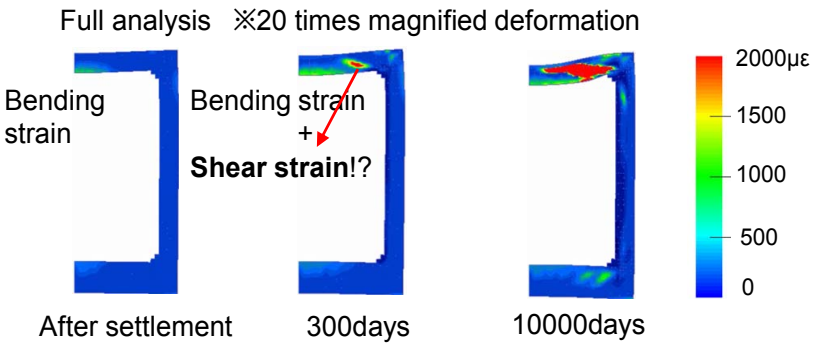

Fig. 21 The shear cracks observed near the haunch in the two dimensional analysis.

soil properties and ground structures, it is thought to be within the tolerance.

It is thought that some highly nonlinear event might take place at the turning point of about 300-500 days. For clarifying the trigger of the following high nonlinearity, the strain field of out-of-plane section is shown in **Fig. 21**. Just after the settlement of the backfill soil, mode of deformation is flexure and bending crack zone can be seen on the bottom face near the span center of the top slab. But, this mode of deformation suddenly shifts to out-of-plane shear accompanying the diagonal cracking as shown in **Fig. 21**. Afterwards, shear deformation proceeds more and more, and the internal inclined shear crack is further propagating. Under this situation, deflection is going on without yield of main reinforcement.

Here, we have a tentative conclusion that the excessive deflection would be attributed to the "delayed shear failure". Let us direct our attention again to the strain of main reinforcement for the cases of IV and II as shown

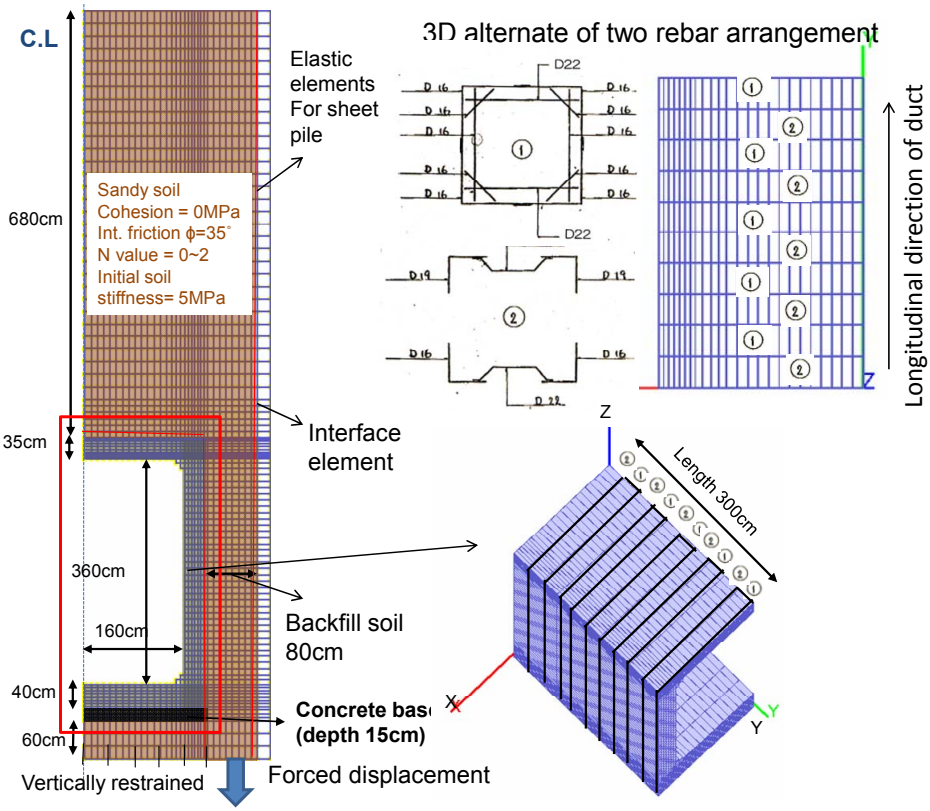

Fig. 22 Three-Dimensional FE model of underground RC culvert.

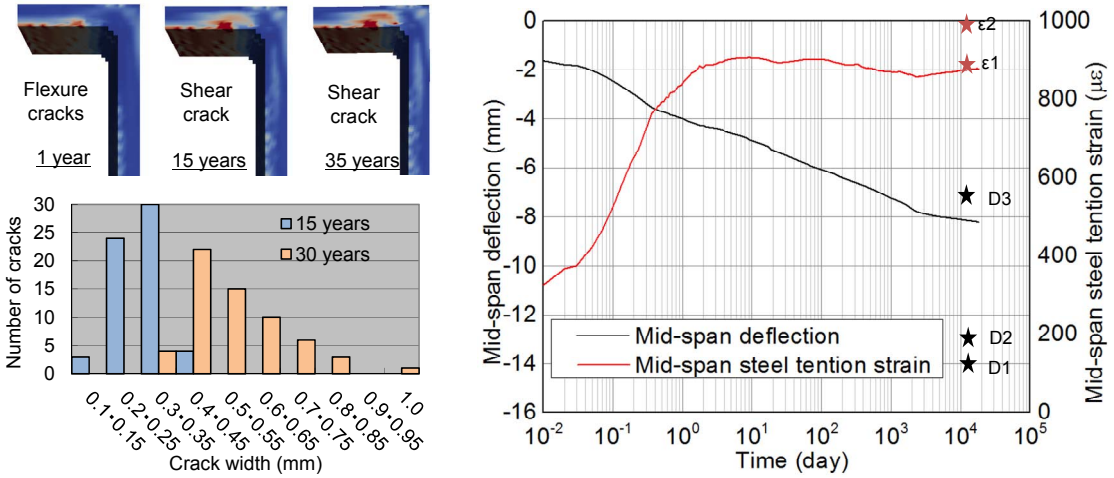

Fig. 23 Contour of the maximum principle strains and mid-span deflection in time domain.

in **Fig. 19**. The strain of main reinforcement at the span center is almost similar. Thus, the flexural deflection based upon in-plane mode is thought to be similar as well. But, the overall deflection is much different. Only possible explanation is that the displacement component of out-of-plane shear is different. This is "shear failure".

The authors also checked the effect of 3D stress field in more detail by using the FE mesh as shown in **Fig. 22**. The arrangement of reinforcing bars in the longitudinal direction of the culvert is exactly reproduced. The reinforcement ratio defined in the 2D analysis (**Fig. 17**) is the averaged one of reinforcing bars along the axis of the culvert (**Fig. 22**). The stress of main reinforcement and the deflection are similar to the 2D analysis at the span center as shown in **Fig. 23**. The displacement of 3D analysis at 30 years is a bit smaller in comparison with those of 2D analysis having sharper localization of the shear failure zone, because the diagonal shear crack band is a little blunt due to non-uniform pattern of the reinforcement arrangement and the interactiofhn of shear crack band of 3D extent along the axis of the duct. Anyhow, the delayed diagonal shear crack propagation is the key factor of the excessive deflection.

Figure 24 shows the computed mean sectional shear force over time. For the full nonlinear coupling analysis, the computed shear force is kept almost constant and

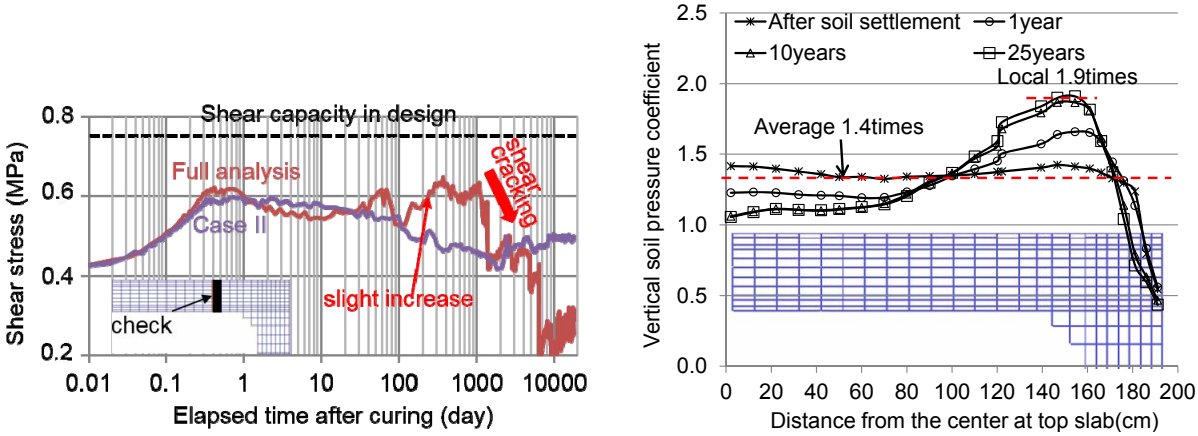

Fig. 24 Profile of the vertical earth pressure and correponding sectional shear force.

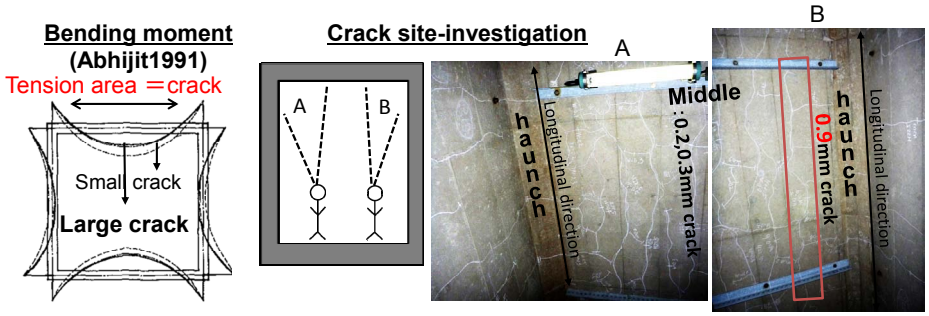

Fig. 25 Site inspections of problematic cracks near the corner of the box section.

about 80~90% of the static shear capacity estimated by the shear design formulae (JSCE 2012). Then in computation, the shear failure of the section takes place under the sustained shear force which does not reach the instantaneous static capacity. As stated previously, the diagonal shear crack starts to appear in the analysis at about 300 days and extends over the depth of the top slab for the next several years. At this moment, drying of moisture in concrete has been almost finished.

As shown in **Fig. 24**, the sectional mean shear stress is decayed after the shear failure. But, the soil-RC system is kept stable owing to the interaction. After the shear cracking, the vertical soil pressure around the span center of the top slab is definitely decreased, and the centroid of the soil pressure shifts (Dasgupta and Sengupta 1991) to the corner of high stiffness. Thus, the delayed shear failure under sustained shear force is thought to be caused mainly by the time-dependent crack propagation, i.e., "mechanistic" delayer shear failure, which shall be confirmed experimentally in the following chapter.

5. Out-of-plane shear failure and its detection

In the previous sections, out-of-plane shear failure is assumed to be associated with the excessive deflection based upon both the integrated analyses and the site monitoring. Then, it is very critical to prove the presence of out-of-plane shear cracks. But, geometrically, the shear crack which may develop within the web zone of the slabs and the walls cannot be seen from inside of the tunnels and utility ducts as shown in **Fig. 25**. The out-of-plane shear failure always accompanies the diagonal cracks which may produce the transverse gap on the surface of members. On the contrary, the flexural cracks are introduced normal to the axis of the members, and just the flat opening mode arises as shown in **Fig. 26**.

The authors illuminated the slab surface laterally, and could find the shadow, which may not be made by the flat opening of flexure cracks but produced by the transverse gap of the shear cracking. When we touch and trace the surface by fingers, it is also easy to recognize the shear crack having the transvers gap in out-of-plane motion. As for the non-destructive testing to detect the shear cracking, this illumination method will be useful especially in dark spaces.

Finally, the authors conducted the destructive testing to directly observe the shear crack planes by digging several bore-holes as shown in **Fig. 27**. The core samples and the mark of crack planes were obtained and their extension exhibits the inclined crack pattern as shear. Here, the presence of the diagonal shear crack and the out-of-plane failure zone is demonstrated. The close-up of the 3D nonlinear analysis around the corner of the duct (see **Fig. 23**) is added in **Fig. 27**. The location of the major shear crack zone accompanying the greatest surface crack opening and the shear gap roughly coincides with the 3D analysis. As stated in the pre-

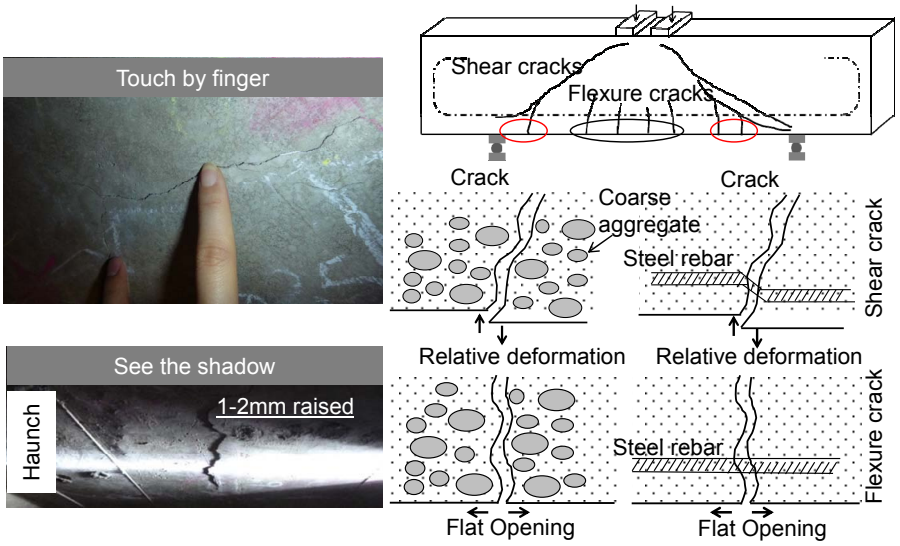

Fig. 26 Illuminating detection of shear cracks.

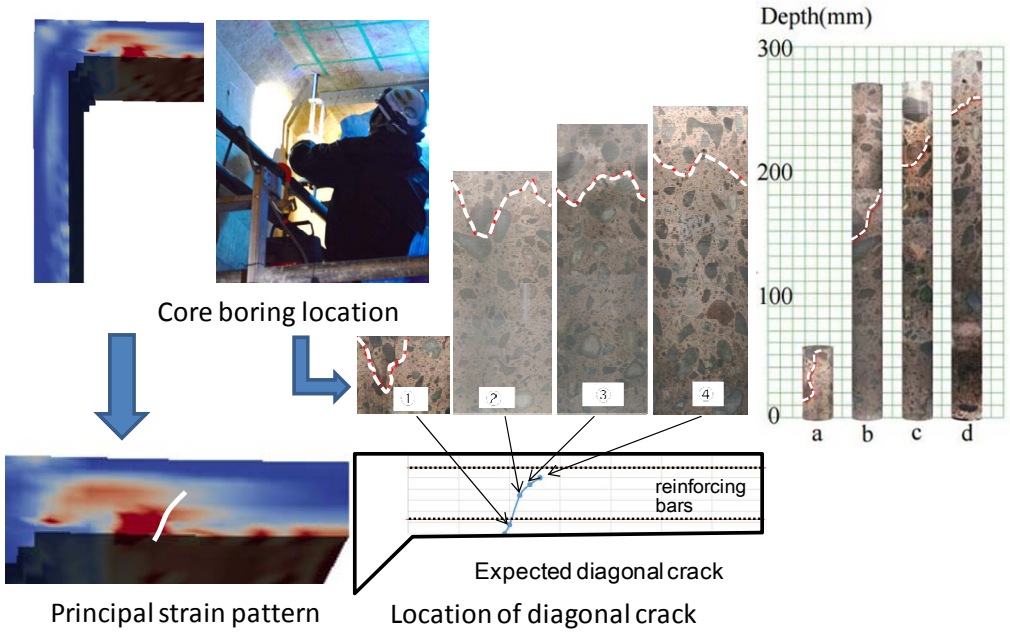

Fig. 27 Image of the inner surface of the bore-hole and detected diagonal shear crack.

vious section, the secondary blunt shear band is seen in the analysis. Then, some other shear crack(s) might exist near by the identified crack at site.

The analytical discussion is firmly supported by these circumstantial evidences. There are some other reports on the out-of-plane failure of underground concrete members such as the concrete invert for tunnels located in deep rocks (Maruyama 2013). But in this paper, the discussion is focused on the shallow underground utility ducts under differential shrinkage and the instability of foundation.

6. Delayed shear failure of RC beams under sustained loads

The integrated modelling used in this study has been already verified regarding the reduced shear capacity of drying RC members (Gebreyouhannes *et al.* 2014). Then, this drying effect of structural concrete is implicitly taken into account in the shear failure simulation as shown in **Fig. 24.** But in this verification, the loading rate of shear was rather rapid than the case of this study. The delayed shear failure simulation of the culvert is the case where the load is rather sustained. Then, in this chapter, the authors try to examine the case where the shear failure occurs under the sustained shear forces.

The multi-scale integrated analysis (Maekawa *et al.* 2008, Yoneda *et al.* 2014, Gebreyouhannes *et al.* 2014) used in this study brings about the delayed shear failure computationally as shown in **Fig. 28**. When 80% of the short-term shear capacity is kept loaded, the diagonal cracks gradually propagate and finally, instability of

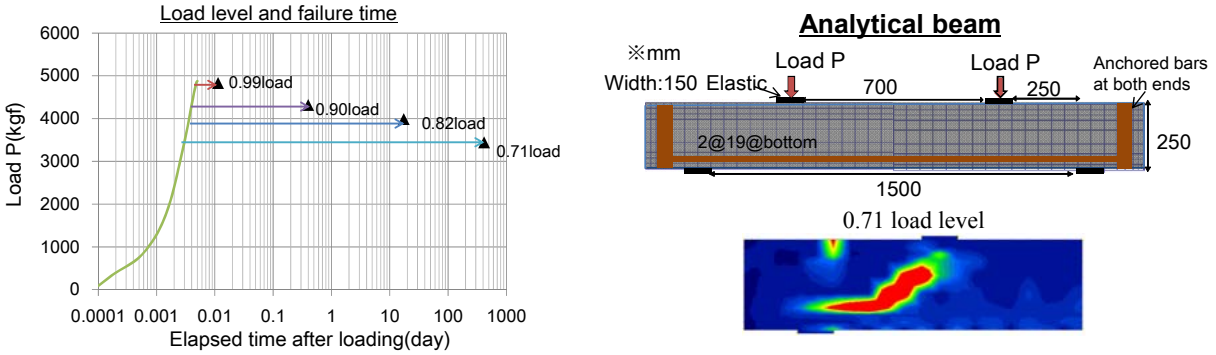

Fig. 28 Computed delayed shear failure under different sustained loads.

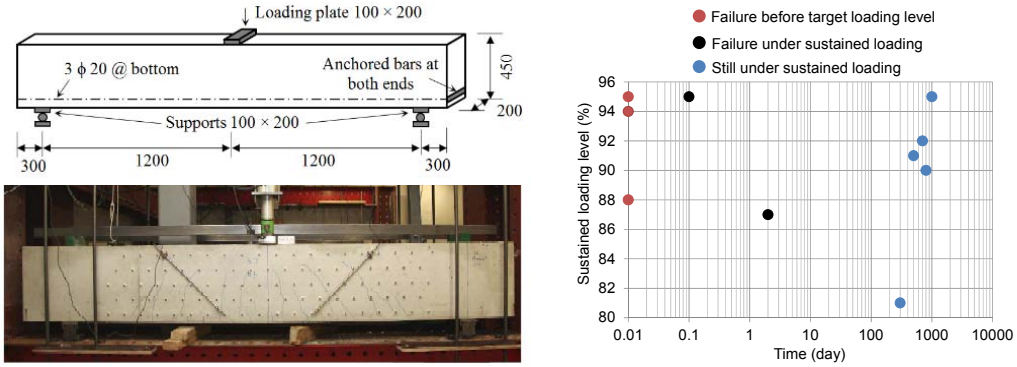

Fig. 29 Sustained shear experiment and delayed failure (Sarkhosh *et al*. 2013).

crack propagation causes member failure at about 100 days as shown in **Fig. 28**. As a matter of fact, almost the constant shear force of about 80% of the short-term static one was being applied (see **Fig. 24**) and reached the failure at about 300 days. When the sustained load level is raised, the period of life to failure is exponentially reduced. This trend computed for delayed shear is most similar to the creep rupture's life of concrete in compression (Rusch 1960).

Sarkhosh *et al*. (2013) carried out the valuable experiments of RC beams subjected to constant loads of different magnitude as shown in **Fig. 29**. The delayed shear failure was reported. Here, the relation of the shear force and corresponding life time till failure was not clear. As a matter of fact, deviation of experimentally obtained short-term shear capacity of RC beams is about 10% around the mean value. Then, it is logically hard to identify the response under 90% of the static capacity with small numbers of specimens. In other words, the exact short-term shear capacity cannot be identified before the experiment. Then in some cases, the failure happened before the target load level which was estimated beforehand. It actually happens that the estimated target loads could be more than the real static capacity, especially when the target level is rather close to the potential capacity.

Piseth *et al*. (2014) conducted the shear loading test where the persistent shear force was applied and its magnitude was increased step by step according to the diagonal crack propagation monitored periodically. Finally, the propagation of a diagonal crack under the sustained shear force was observed. Here, the different shear crack paths were also reported when the load-time path was changed. Since the time till failure was about a week, the progress of the drying shrinkage is estimated to be less. Thus, it can be concluded again that the delayed shear failure or creep rupture may occur under constant loads. The point of discussion is how long RC beams can actually bear the constant high shear force.

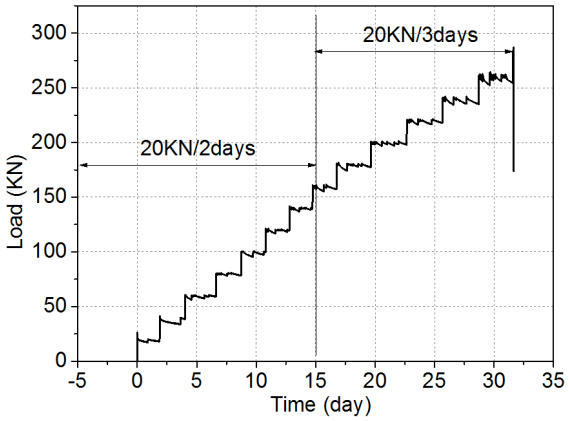

Fig. 30 Stepwise sustained loading in experiment.

In considering the experimental and analytical background stated previously, the authors introduced the step-wise loading pattern as shown in **Fig. 30** and **Table 6** to the simply supported RC beam (see **Fig. 31**). The shear span to depth ratio of the RC beam was decided so that it may roughly fit the kinematics of foreseen combined sectional forces around the corner of the culvert.

Table 6 Stepwise loading history.

Step	1	2	3	4	5	6	7	8	9	10	11	12	13	14
Sustained time (days)	1.9	2.2	2.6	2.1	2.0	2.0	2.0	2.0	2.9	3.0	3.0	3.1	2.8	0.1
Average loading increase (KN)	18.7	17.4	22.8	20.6	18.7	20.9	20.0	19.1	20.2	20.4	20.1	18.8	19.9	22.5

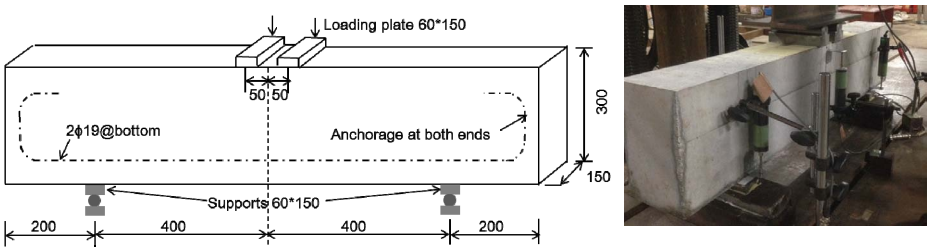

Fig. 31 Geometry of the RC beams (left) and measurement devices installed on the beam (right).

Table 7 Mix proportion of concrete.

W/C (%)	water (kg/m^3)	cement (kg/m^3)	gravel (kg/m^3)	sand (kg/m^3)	air (%)
40	170	425	950	760	4.5

Table 8 Properties of materials.

concrete compressive strength (N/mm^2)	concrete tensile strength (N/mm^2)	steel yield strength (N/mm^2)	bending failure load (KN)	shear failure load (KN)
57.3 (36days)	3.48 (39days)	450	285	275

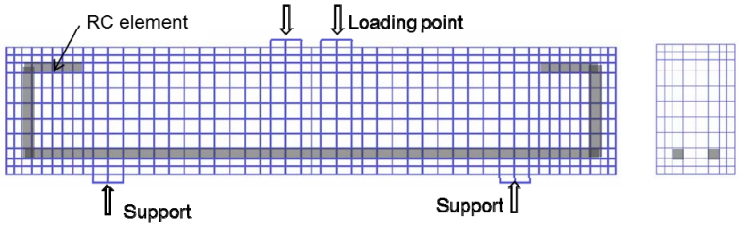

Fig. 32 FE model of the delayed shear experiment of RC beam.

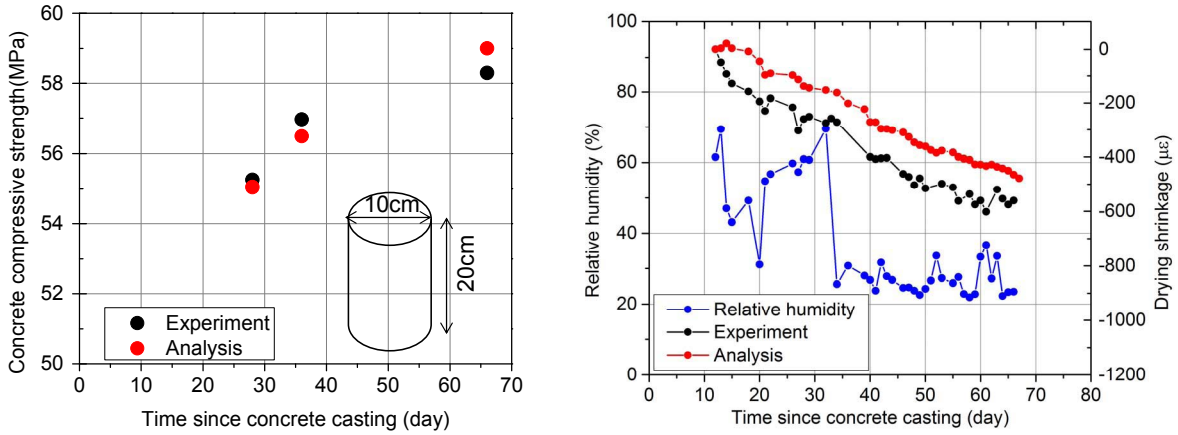

Fig. 33 Computed and experimentally obtained compressive strength of cylinder and mean drying shrinkage of the standard specimen subjected to the ambient relative humidity in laboratory.

Originally, this method of step-wise uplift of loads has been used in experiments for the high cycle fatigue life of RC and PC bridge deck slabs. In this study, first, the middle-level constant load was applied for two or three days as shown in **Fig. 30.** If no failure takes place, the sustained load level was slightly raised, and we may wait for the failure. If not, we go to the next stage. Then, we can roughly obtain the load level which causes delayed shear failure to take 2~3 days till failure.

Figure 31 shows the experimental set-up, and the deflection was measured under the step-wise load as shown in **Fig. 30**. The mix proportion of concrete used

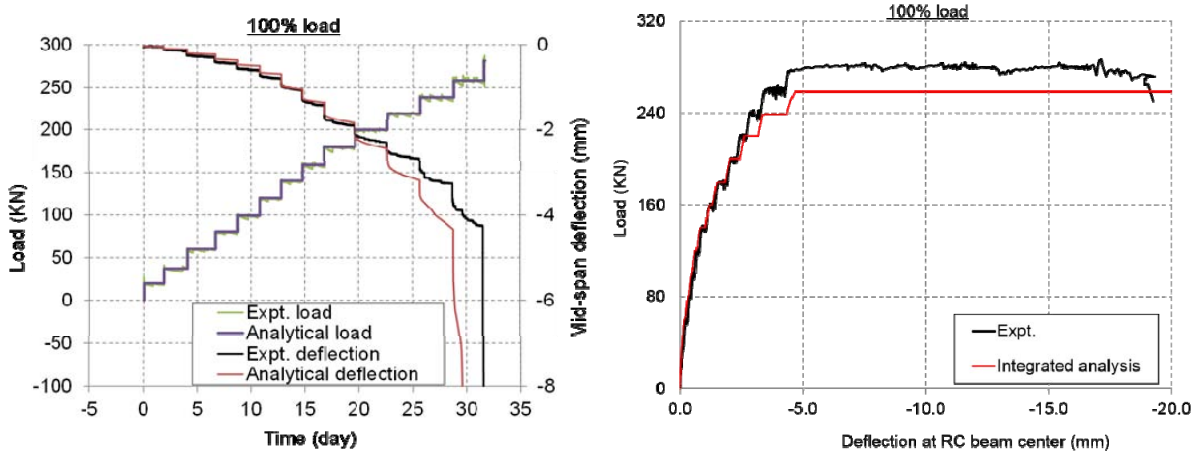

Fig. 34a Applied load of 100% magnitude and corresponding deflection versus time.

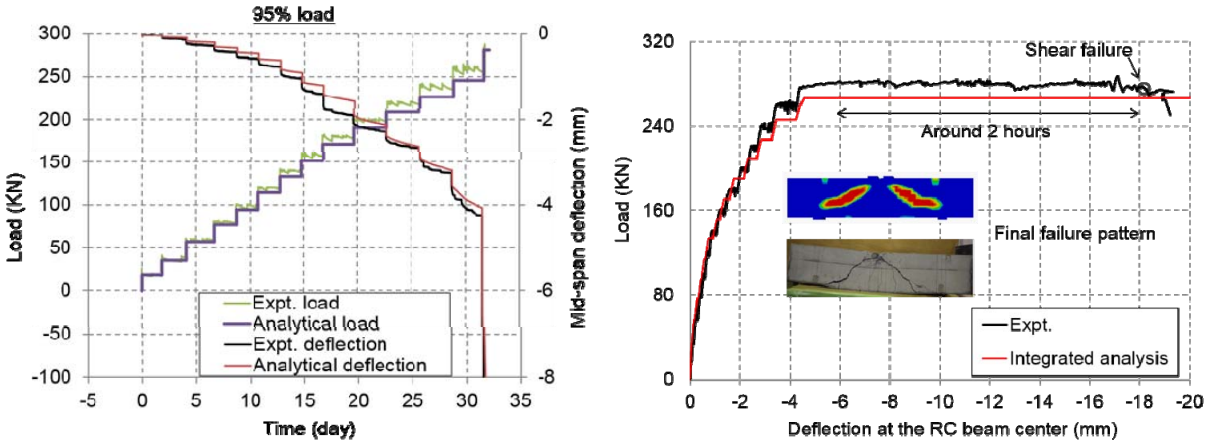

Fig. 34b Applied load of 95% magnitude and corresponding deflection versus time.

for the input data of the thermo-hygral integrated analysis is listed in **Table 7**. The FE discretization is shown in **Fig. 32** according to the dimensioning of the experiment. The wet curing was continued till 11 days after casting of fresh concrete.

During this period of wet curing, the cement hydration in concrete, the micro-structure formation and strength development were simulated under no external force. The shrinkage deformation driven by the capillary forces and disjoining pressure was computed after 11 days of wet curing by the integrated analysis (Yoneda *et al*. 2013, 2015, Maekawa *et al*. 2008). Here, the room temperature was 20 degree Celsius and the relative humidity was 60%. **Figure 33** shows the strength development of the cylinder specimen in uniaxial compression, and the averaged drying shrinkage of the standard specimen. The computed results by the integrated analysis do not deviate from the reality. The step-by-step loading started at 36days after mixing, and the corresponding displacement at the span center of the top slab and the load-displacement relation are indicated in **Fig. 34a**. At the loading from 240kN, the shear failure suddenly took place before keeping the load at the higher level.

Since the reproducibility of the shear capacity is

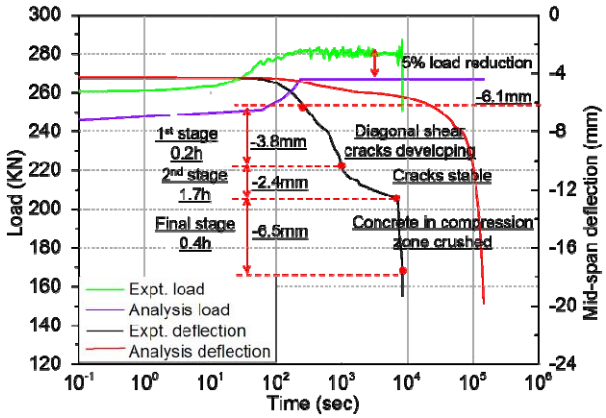

Fig. 35 Three stages of creep deflection under sustained loads just before the final shear failure.

about 10% around the mean value (Okamura and Higai 1980) based upon about two thousands specimens, the authors re-computed the response under 95% mechanistic action of the experimentally applied load as shown in **Fig. 34b**. The relation of load-deflection and the transient displacement with regard to time fairly follow up the experiment. **Figure 35** is the close-up of the progressive deflection of the top slab under the sustained force

(95% in **Fig. 34b**) just before the collapse. The delayed shear failure certainly took about 2.3 hours under the 270kN, and the computation predicts about 2hours from 6mm to 18mm deflection in progress. Since the estimated short-term shear capacity is 275kN (JSCE 2012), the observed delayed shear failure of about 2 hours will correspond to about 90% of the static capacity.

If the period of load suspension at each progressive step would be 10 days or 100 days, we will be able to have the level of shear force corresponding to each period of life till failure. Thus, this study does not encompass the whole figure of delayed shear failure, but merely examines the short-term delayed shear failure and the partial verification of the integrated analysis. The delayed shear failure under middle and/or lower levels of sustained loads will be clarified in future works.

7. Conclusions

In conjunction with the site inspection and monitoring, laboratory experiments and multi-scale integrated analyses, the mechanism of the excessive deflection and the out-of-plane shear failure of real underground box culverts were investigated, and the following conclusions are earned.

(1) The out-of-plane diagonal shear cracks were found near the corner of shallow underground RC box culverts in service, and the excessive deflection which is more than 10times the design deflection was recognized.
(2) The shear cracks appearing under the top slabs were detected by the illuminating technique as well as the destructive testing with bore holes. According to the past monitoring of cracks from inside of the culvert, its width and the absolute extension of cracking was increasing in the past three decades.
(3) The thermo-hygral multi-scale analysis was used for behavioural simulation of the soil-RC culvert system from the construction to the current state. Then, computationally reproduced are the transient extension of the shear crack, the delayed failure and the large excessive deflection of the culvert.
(4) The sensitivity analyses was systematically carried out in terms of i) subsidence of the backfill soil foundation, ii) differential shrinkage, and iii) sustained higher stress causing creep and transient crack propagation. It is found that coupling of all three factors lead to the excessive deflection with delayed shear failure. The delayed shear failure cannot be explained by only one factor.
(5) The delayed shear failure under sustained load less than the maximum shear capacity was proved by the experiment and the numerical analysis was partially verified.

Acknowledgements

The authors express their sincere gratitude to Prof. R. Kuwano of The University of Tokyo, Dr. E. Gebreyouhannes of Addis Ababa University, Mr. M. Kunieda of Graduate School of the University of Tokyo, Dr. T. Mishima of Maeda Corporation, Dr. Y. Hiratsuka of Sho-bond Corporation for their valuable advices and suggestions. This paper was financially supported by MEXT/JSPS KAKENHI 23226011.

References

Abhijit, D. and Bratish, S., (1991). "Large-scale model test on square box culvert backfilled with sand." ASCE, *Journal of Geotechnical Engineering*, 117(1), 156-161.

Asamoto, S., Ishida, T. and Maekawa, K., (2006). "Time-dependent constitutive model of solidifying concrete based on thermodynamic state of moisture in fine pores." *Journal of Advanced Concrete Technology*, 4(2), 301-323.

Bang, D. P. D., Benedetto, H. D., Duttine, A. and Ezaoui, A., (2007). "Viscous behaviour of dry sand." *International Journal for Numerical and Analytical Methods in Geomechanics*, 31(15), 1631-1713.

Bažant, Z. P., Yu, Q., Li, G. H., Klein, G. J. and Krístek, V., (2010). "Excessive deflections of record-span prestressed box girder - Lessons learned from the collapse of the Koror-Babeldaob Bridge in Palau." *Concrete International*, ACI, 32, 44.

Bazant, Z. P., (2001). "Prediction of concrete creep and shrinkage: past, present and future." *Nuclear Engineering and Design*, 203(1), 27-38.

Bennett, R., Wood S., Drumm, E. and Rainwater, N., (2005). "Vertical loads on concrete box culverts under high embankments." *Journal of Bridge Engineering*, 10(6), 643-649.

Chijiwa, N., Zhu, X., Ohno, H., Tanabe, S., Nakarai, K. and Maekawa, K., (2015). "Delayed shear crack formation of shallow RC box culverts in service." In: C. Hellmich, B. Pichler and J. Kollegger, Eds. CONCREEP 10, *Mechanics and Physics of Creep, Shrinkage and Durability of Concrete and Concrete Structures*, 1579-1586.

Dasgupta, A. and Sengupta, B., (1991). "Large-scale model test on square box culvert backfilled with sand." *Journal of Geotechnical Engineering,* 117, 156-161.

Gebreyouhannes, E., Yoneda, T., Ishida, T. and Maekawa, K. (2014). "Multi-scale based simulation of shear critical reinforced concrete beams subjected to drying." *Journal of Advanced Concrete Technology*, 12(10), 363-377.

Gilbert, R. I., (1999). "Deflection calculation for reinforced concrete structures: why we sometimes get it wrong." *ACI Structural Journal*, 96(6), 1027-1032.

Guo, X. and Gilbert, R. I., (2002). "An experimental study of reinforced concrete flat slabs under sustained service loads." *UNICIV Report* R-407.

Gutierrez, M., Ishihara, K. and Towhata, I., (1993). "Model for the deformation of sand during rotation of principal stress directions." *Soils and Foundations*, 33(3), 105-117.

Japan Society of Civil Engineers, (2012). "*Standard*

Specification of Concrete Structures (Design)." JSCE, Maruzen, Tokyo.

Kunieda, M., Zhu, X., Nakajima, Y., Tanabe, S. and Maekawa, K., (2014). "Long-term serviceability and risk assessment of shallow underground RC culverts and tunnels." In: K. van Breugel and E. A. B. Koenders, Eds. *Proceedings of the 1st Ageing of Materials & Structures*, The Netherland, 376-383.

Kuwano, R. and Ebizuka, H., (2010). "Trapdoor tests for the evaluation of earth pressure acting on a buried structure in an embankment." In: *Proceeding of the 9th International Symposium on New Technologies for Urban Safety of Mega Cities in Asia,* USMCA, Kobe.

Lade, P. and Liu, C., (1998). "Experimental study of drained creep behavior of sand." *Journal of Engineering Mechanics*, ASCE, 124(8), 912-920.

Maekawa, K., Ishida, T. and Kishi, T., (2008). "*Multiscale Modeling of Structural Concrete*." Taylor & Francis.

Maekawa, K. and Fukuura, N., (2014). "*Nonlinear modeling of 3D structural reinforced concrete and seismic performance*." In: Thomas T. C. Hsu, ed. *Infrastructure Systems for Nuclear Energy*, John Wiley & Sons.

Maekawa, K. and Ishida, T., (2002). "Modeling of structural performances under coupled environmental and weather actions." *Materials and Structures*, 35, 591-602.

Maruyama, K., (2007). "Damage investigation of Tarui highway PRC bridge: What happened and what we should do in design and construction in practice." *Cement and Concrete*, 725, 14-18 (in Japanese).

Maruyama, M., (2013). "Rebuild invert concrete through continuous 61-day Lane-Closure, -Joshin-etsu Expressway Nikkure-yama Tunnel-." *Tunnels and Underground*, 44(12), 17-28. (in Japanese)

Mitani, T., Hyodo, H., Ota, K. and Sato, R., (2011). "Discover and the evaluation of shear strength decrease of reinforced normal-strength concrete beams." *Proceedings of Japan Concrete Institute*, 33(2), 721-726. (in Japanese)

Moshirabadi, S., Soltani, M. and Maekawa, K., (2015). "Seismic interaction of underground RC ducts and neighboring bridge piers in liquefiable soil foundation." *Acta Geotechnica*, 10(6), 761-780.

Ohno, M., Chijiwa, N., Suryanto, B. and Maekawa, K., (2012). "An investigation into the long-term excessive deflection of PC viaducts by using 3D multi-scale integrated analysis." *Journal of Advanced Concrete Technology*, 10, 47-58.

Okamura, H. and Higai, T., (1980). "Proposed design equation for shear strength of reinforced concrete beams without web reinforcement." *Proceedings of Japan Society of Civil Engineers*, 300, 131-141.

Osada, K., Ono, K., Maruya, T. and Ikeda, S., (2006). "Seismic performance of concrete piers deteriorated by alkali silica reaction." *Concrete Journal*, 44(3), 34-42 (in Japanese).

Pickett, G., (1942). "The effect of change in moisture-content on the creep of concrete under a sustained load." *Journal of American Concrete Institute*, 38, 333-356.

Piseth, V., Nakarai, K., Chijiwa, N. and Maekawa, K., (2015). "Experimental study on the effects of a loading rate on the shear performance of an RC beam." *CONCREEP 10, Mechanics and Physics of Creep, Shrinkage and Durability of Concrete and Concrete Structures*, ASCE, 1561-1569.

Rusch, H., (1960). "Research towards a general flexural theory for structural concrete." *Journal of the ACI*, 57(1), 1-27.

Salem, H. and Maekawa, K., (1999). "Spatially averaged tensile mechanics for cracked concrete and reinforcement under highly inelastic range." *Journal of Materials, Concrete Structures and Pavements*, V-42(613), 277-293.

Sarkhosh, R., Walraven, J., den Uijl, J. and Braam, R., (2013). "Shear capacity of concrete beams under sustained loading." IABSE Symposium Report, 99, 162-169.

Schabowicz, K. and Hola, J., (2012). "Nondestructive elastic-wave tests of foundation slab in office building." *Materials Transactions*, Special Issue on APCNDT 2009, 53(2), 296-302.

Siddiquee, M. S. A., Tatsuoka, F. and Tanaka, T., (2006). "FEM Simulation of the viscous effects on the stress-strain behaviuour of sand in plane strain compression." *Soils and Foundations*, 46(1), 99-108.

Soltani, M. and Maekawa, K., (2015). "Numerical simulation of progressive shear localization and scale effect in cohesionless soil media." *International Journal of Non-Linear Mechanics*, 69(March), 1-13.

Tadros, M. K. and Benak, J. V., (1989). "Soil pressure on box culverts." *ACI Structural Journal*, 86(4), 439-450.

Towhata, I. and Ishihara, K., (1985a). "Undrained strength of sand undergoing cyclic rotation of principal stress axis." *Soils and Foundations*, 25(2), 135-147.

Towhata, I. and Ishihara, K., (1985b). "Modeling soil deformation undergoing cyclic rotation of principal stress axes." In: *Proceeding of 5th International Conference on Numerical Method in Geomechanics*, Nagoya, Japan, 523-530.

Vecchio, F. and Collins, M. P., (1986). "The modified compression-field theory for reinforced concrete element subjected to shear." *ACI Journal*, March-April, 219-231.

Woodbury, W. H., Bayer, E. J., Botts, A. E., Daley, C. A., Pettus, J. K. and Wilks, J. R., (1926). "Corrugated metal culverts for railroad purposes." Preparing specifications, with assistance of committee on iron and steel structures, *Bull. Am. Railway Eng. Assoc.*, 27(284), 794-828.

Yoneda, T., Ishida, T., Maekawa, K., Gebreyouhannes, E. and Mishima, T., (2015). "A micro-cracking model coupled with micro fracture and water status in micro

pore structures." *Journal of Japan Society of Civil Engineers,* E2 (*Materials and Concrete Structures*), 71(3), 263-282.

Yoneda, T., Ishida, T., Maekawa, K., Gebreyouhannes, E. and Mishima, T., (2013). "Simulation of early-age cracking due to drying shrinkage based on a multi-scale constitutive model." *Poromechanics V*: ASCE, 579-588.

Zhu, X., Kunieda, M., Nakajima, Y., Tanabe, S. and Maekawa, K., (2014). "Long-term serviceability and delayed shear failure risk assessment of shallow underground RC culverts." In: J. Sim Ed., *The 6th International Conference of Asian Concrete Federation,* Seoul.